Numerical study of 1+1D drift kinetic model with wall boundary conditions

M. Barnes[1], F. I. Parra[1], M. R. Hardman[1] and J. Omotani[2]

[1] Rudolf Peierls Centre for Theoretical Physics, University of Oxford, Clarendon Laboratory, Parks Road, Oxford OX1 3PU, United Kingdom

[2] Culham Centre for Fusion Energy, Culham Science Centre, Abingdon, Oxon, OX14 3DB, United Kingdom

E-mail: michael.barnes@physics.ox.ac.uk

1. Introduction

Magnetic field lines beyond the last-closed-flux-surface begin and end on the vessel wall. For these field lines, the periodic boundary condition along the field line employed in our previous numerical treatment of parallel dynamics [1, 2, 3] must be modified. To that end we summarise in this document the numerical algorithm we employ to solve parallel-to-the-field dynamics for a standard, i.e., not moment-based, drift kinetic model with wall boundary conditions. A brief summary of the 1+1D model and the wall boundary conditions is given before describing code normalisation and implementation details. An analytical solution is provided to serve as a code benchmark, and results are presented to demonstrate that the code behaves as expected.

2. Model equations

A detailed derivation of the drift kinetic model we consider is provided in our May 2021 report [4]. For the Reader's convenience we produce an overview of this drift kinetic model, noting any additional simplifying assumptions. The system we consider consists of a single ion species of charge e and mass m_i, a single neutral species of mass $m_n = m_i$, and an electron species modelled as having a Boltzmann response, all immersed in a straight, uniform magnetic field in the z direction. We allow for charge exchange collisions between ions and neutrals and ionization collisions involving ions, electrons and neutrals, but do not account for intra-species collisions. Finally, we assume that the plasma is homogeneous in the plane perpendicular to the magnetic field. With these assumptions, our model system of equations is

$$\frac{\partial f_i}{\partial t} + v_\parallel \frac{\partial f_i}{\partial z} - \frac{e}{m_i}\frac{\partial \phi}{\partial z}\frac{\partial f_i}{\partial v_\parallel} = -R_{\rm in}\left(n_n f_i - n_i f_n\right) + R_{\rm ion} n_e f_n, \tag{1}$$

$$\frac{\partial f_n}{\partial t} + v_\parallel \frac{\partial f_n}{\partial z} = -R_{\rm in}\left(n_i f_n - n_n f_i\right) - R_{\rm ion} n_e f_n, \tag{2}$$

$$n_s(z,t) = \int_{-\infty}^{\infty} dv_\parallel f_s(z, v_\parallel, t), \tag{3}$$

and

$$n_i = n_e = N_e \exp\left(\frac{e\phi}{T_e}\right), \tag{4}$$

with $f_s \doteq \int d\vartheta dv_\perp v_\perp F_s$ the marginalized particle distribution function for species s, $v_\parallel$ and $v_\perp$ the components of the particle velocity parallel and perpendicular to the magnetic field, respectively, ϑ the gyro-angle, t the time, ϕ the electrostatic potential, and R_{in} and R_{ion} charge exchange and ionization collision frequency factors.

2.1. Wall BCs

Complicated dynamics can occur very close to the wall, leading to a hierarchy of narrow layers with different dynamics. Derivation of the equations that describe these 'sheaths' is an ongoing research activity in the magnetic confinement fusion community. We avoid such complications here by considering a plasma domain whose boundaries in z are the entrances to the sheaths furthest from the wall.

Ions that exit the simulation domain are assumed to continue on to the wall, where they recombine. As a result, no ions enter the domain from the walls, giving a zero incoming BC for the ions:

$$F_i(z = 0, v_\parallel > 0, v_\perp, t) = 0 = F_i(z = L_z, v_\parallel < 0, v_\perp, t). \tag{5}$$

Neutrals that leave the domain are assumed to hit the wall and thermalise at the temperature of the wall, T_w. Ions that recombine at the wall also re-enter as neutrals. The resulting boundary condition on the neutrals is

$$F_n(z = 0, v_\parallel > 0, v_\perp, t) = \Gamma_0 F_{Kw}(v_\parallel, v_\perp), \quad F_n(z = L_z, v_\parallel < 0, v_\perp, t) = \Gamma_{L_z} F_{Kw}(v_\parallel, v_\perp), \tag{6}$$

where

$$F_{Kw}(v_\parallel, v_\perp) \doteq \frac{3}{\pi}\left(\frac{m_i}{2T_w}\right)^2 \frac{\left|v_\parallel\right|}{\sqrt{v_\parallel^2 + v_\perp^2}} \exp\left(-\frac{m_i\left(v_\parallel^2 + v_\perp^2\right)}{2T_w}\right) \tag{7}$$

is the Knudsen cosine distribution, and

$$\Gamma_0 \doteq \sum_{s=i,n} 2\pi \int_{-\infty}^{0} dv_\parallel \int_0^{\infty} dv_\perp v_\perp \left|v_\parallel\right| F_s(z = 0, v_\parallel, v_\perp, t) \tag{8}$$

and

$$\Gamma_{L_z} \doteq \sum_{s=i,n} 2\pi \int_{0}^{\infty} dv_\parallel \int_0^{\infty} dv_\perp v_\perp \left|v_\parallel\right| F_s(z = L_z, v_\parallel, v_\perp, t) \tag{9}$$

are the combined fluxes of neutrals and ions towards the walls at $z = 0$ and $z = L_z$, respectively.

We next marginalise the above distribution functions by integrating over gyro-angle and $v_\perp$ to get

$$f_i(z=0, v_\parallel > 0, v_\perp, t) = 0 = f_i(z=L_z, v_\parallel < 0, v_\perp, t) \tag{10}$$

and

$$f_n(z=0, v_\parallel > 0, t) = \Gamma_0 f_{Kw}(v_\parallel), \quad f_n(z=L_z, v_\parallel < 0, t) = \Gamma_{L_z} f_{Kw}(v_\parallel), \tag{11}$$

with

$$f_{Kw}(v_\parallel) \doteq 2\pi \int_0^\infty dv_\perp v_\perp F_{Kw}(v_\parallel, v_\perp) = 3\sqrt{\pi}\left(\frac{m_i}{2T_w}\right)^{3/2} \left|v_\parallel\right| \operatorname{erfc}\left(\sqrt{\frac{m_i}{2T_w}}\left|v_\parallel\right|\right) \tag{12}$$

and erfc the complementary error function. The fluxes toward the wall at the domain boundaries can be recast in terms of the marginalised distribution function:

$$\Gamma_0 = \sum_{s=i,n} \int_{-\infty}^0 dv_\parallel \left|v_\parallel\right| f_s(z=0, v_\parallel, t) \tag{13}$$

and

$$\Gamma_{L_z} = \sum_{s=i,n} \int_0^\infty dv_\parallel \left|v_\parallel\right| f_s(z=L_z, v_\parallel, t). \tag{14}$$

2.2. Density evolution

If we consider the evolution of the line-averaged species densities, $\overline{n}_s$, we obtain

$$\frac{\partial \overline{n}_s}{\partial t} = \frac{1}{L_z}\left(\Gamma_s(z=0) - \Gamma_s(z=L_z)\right) \pm R_{\text{ion}} \overline{n_i n_n}, \tag{15}$$

with the + and - signs corresponding to ions and to neutrals, respectively. For the ions

$$\Gamma_i(0) = \int_{-\infty}^0 dv_\parallel v_\parallel f_i(z=0, v_\parallel) < 0, \tag{16}$$

and

$$\Gamma_i(L_z) = \int_0^\infty dv_\parallel v_\parallel f_i(z=L_z, v_\parallel) > 0, \tag{17}$$

where we have used the boundary conditions on f_i given by expression (10).

For the neutrals

$$\begin{aligned} \Gamma_n(0) &= \int_{-\infty}^0 dv_\parallel v_\parallel f_n(z=0, v_\parallel) + \Gamma_0 \int_0^\infty dv_\parallel v_\parallel f_{Kw}(v_\parallel) \\ &= \int_{-\infty}^0 dv_\parallel v_\parallel f_n(z=0, v_\parallel) + \Gamma_0, \end{aligned} \tag{18}$$

and

$$\begin{aligned} \Gamma_n(L_z) &= \int_0^\infty dv_\parallel v_\parallel f_n(z=L_z, v_\parallel) + \Gamma_{L_z} \int_{-\infty}^0 dv_\parallel v_\parallel f_{Kw}(v_\parallel) \\ &= \int_0^\infty dv_\parallel v_\parallel f_n(z=L_z, v_\parallel) - \Gamma_{L_z}, \end{aligned} \tag{19}$$

where we have used the boundary conditions on f_n given by expression (11) and the fact that $\int_0^\infty dv_\parallel v_\parallel f_{Kw} = -\int_{-\infty}^0 dv_\parallel v_\parallel f_{Kw} = 1$.

Combining the results for the ion and neutral densities and noting that the ionization contributions to the ion and neutral densities cancel, we obtain a constraint on the evolution of the total (species-summed), line-averaged density:

$$\begin{aligned}\frac{\partial}{\partial t}\sum_{s=i,n}\overline{n}_s &= \frac{1}{L_z}\sum_{s=i,n}\left(\Gamma_s(z=0)-\Gamma_s(z=L_z)\right)\\ &= \frac{1}{L_z}\left(\sum_{s=i,n}\int_{-\infty}^0 v_\parallel f_s(z=0,v_\parallel)+\Gamma_0-\sum_{s=i,n}\int_0^\infty v_\parallel f_s(z=L_z,v_\parallel)+\Gamma_{L_z}\right)\\ &= \frac{1}{L_z}\left(-\Gamma_0+\Gamma_0-\Gamma_{L_z}+\Gamma_{L_z}\right)\\ &= 0.\end{aligned} \tag{20}$$

This is a consequence of the assumed wall boundary condition, which dictates that any particles leaving the domain re-enter as neutrals (and thus total density is conserved). It can (and will) be used to test the numerical implementation of the wall boundary condition.

2.3. Normalisation

We normalize Eqs. (1)-(4) by defining

$$\tilde{f}_s \doteq f_s\frac{c_s\sqrt{\pi}}{N_e}, \tag{21}$$

$$\tilde{t} \doteq t\frac{c_s}{L_z}, \tag{22}$$

$$\tilde{z} \doteq \frac{z}{L_z}, \tag{23}$$

$$\tilde{v}_\parallel \doteq \frac{v_\parallel}{c_s}, \tag{24}$$

$$\tilde{n}_s \doteq \frac{n_s}{N_e}, \tag{25}$$

$$\tilde{\phi} \doteq \frac{e\phi}{T_e}, \tag{26}$$

$$\tilde{R}_{\text{in}} \doteq R_{\text{in}}\frac{N_e L_z}{c_s}, \tag{27}$$

and

$$\tilde{R}_{\text{ion}} \doteq R_{\text{ion}}\frac{N_e L_z}{c_s}, \tag{28}$$

with $c_s \doteq \sqrt{2T_e/m_s}$. In terms of these normalised quantities, Eqs (1)-(4) become

$$\frac{\partial \tilde{f}_i}{\partial \tilde{t}} + \tilde{v}_\parallel \frac{\partial \tilde{f}_i}{\partial \tilde{z}} - \frac{1}{2}\frac{\partial \tilde{\phi}}{\partial \tilde{z}}\frac{\partial \tilde{f}_i}{\partial \tilde{v}_\parallel} = -\tilde{R}_{\rm in}\left(\tilde{n}_n \tilde{f}_i - \tilde{n}_i \tilde{f}_n\right) + \tilde{R}_{\rm ion}\tilde{n}_i \tilde{f}_n, \tag{29}$$

$$\frac{\partial \tilde{f}_n}{\partial \tilde{t}} + \tilde{v}_\parallel \frac{\partial \tilde{f}_n}{\partial \tilde{z}} = -\tilde{R}_{\rm in}\left(\tilde{n}_i \tilde{f}_n - \tilde{n}_n \tilde{f}_i\right) - \tilde{R}_{\rm ion}\tilde{n}_i \tilde{f}_n, \tag{30}$$

$$e^{\tilde{\phi}} = \tilde{n}_i = \frac{1}{\sqrt{\pi}}\int_{-\infty}^{\infty} d\tilde{v}_\parallel \tilde{f}_i, \tag{31}$$

and

$$\tilde{n}_n = \frac{1}{\sqrt{\pi}}\int_{-\infty}^{\infty} d\tilde{v}_\parallel \tilde{f}_n. \tag{32}$$

The normalised forms for the wall boundary conditions are

$$\tilde{f}_i\left(\tilde{z}=0, \tilde{v}_\parallel > 0, \tilde{t}\right) = 0 = \tilde{f}_i\left(\tilde{z}=1, \tilde{v}_\parallel < 0, \tilde{t}\right) \tag{33}$$

and

$$\tilde{f}_n\left(\tilde{z}=0, \tilde{v}_\parallel > 0, \tilde{t}\right) = \tilde{\Gamma}_0(\tilde{t})\tilde{f}_{Kw}(\tilde{v}_\parallel), \quad \tilde{f}_n\left(\tilde{z}=1, \tilde{v}_\parallel < 0, \tilde{t}\right) = \tilde{\Gamma}_{L_z}(\tilde{t})\tilde{f}_{Kw}(\tilde{v}_\parallel), \tag{34}$$

where

$$\tilde{f}_{Kw}(\tilde{v}_\parallel) = c_n^2 f_{Kw}(v_\parallel) = \frac{3\sqrt{\pi}}{\tilde{T}_w^{3/2}}\left|\tilde{v}_\parallel\right| \operatorname{erfc}\left(\frac{\left|\tilde{v}_\parallel\right|}{\sqrt{\tilde{T}_w}}\right), \tag{35}$$

$$\tilde{\Gamma}_0(\tilde{t}) = \sum_{s=i,n}\int_{-\infty}^{0} d\tilde{v}_\parallel \left|\tilde{v}_\parallel\right| \tilde{f}_s(\tilde{z}=0, \tilde{v}_\parallel, \tilde{t}), \tag{36}$$

and

$$\tilde{\Gamma}_{L_z}(\tilde{t}) = \sum_{s=i,n}\int_{0}^{\infty} d\tilde{v}_\parallel \left|\tilde{v}_\parallel\right| \tilde{f}_s(\tilde{z}=1, \tilde{v}_\parallel, \tilde{t}), \tag{37}$$

with $\tilde{T}_w \doteq T_w/T_e$.

3. Analytical solution

To derive an analytical solution for the electrostatic potential for our system, we neglect charge exchange collisions and replace the ionization source term appearing in Eq. (1) with a simplified source. In particular, we follow the approach of Ref. [5] and assume that ionization occurs at a constant rate and gives birth to ions with zero parallel velocity. The resulting ion kinetic equation is

$$\frac{\partial f_i}{\partial t} + v_\parallel \frac{\partial f_i}{\partial z} - \frac{e}{m_i}\frac{\partial \phi}{\partial z}\frac{\partial f_i}{\partial v_\parallel} = R_{\rm ion} N_e^2 \delta(v_\parallel), \tag{38}$$

with $\delta(v_\parallel)$ the Dirac delta distribution. With these assumptions, the ion kinetic equation decouples from the kinetic equation for the neutrals and makes the problem tractable.

Ions that are formed at a given spatial location z_0 are accelerated by the parallel electric field setup by the wall BC toward the walls. The parallel speed of this ion after travelling to a location z closer to the wall, $v_\parallel(z)$ is obtained via conservation of energy:

$$\frac{m_i v_\parallel(z)^2}{2} = e\left(\phi(z_0) - \phi(z)\right). \tag{39}$$

In steady-state, the flux of ions with speeds in the range $v_\parallel$ to $v_\parallel + dv_\parallel$ through the location z must equal the rate at which these ions are generated between z_0 and $z_0 + dz_0$:

$$v_\parallel(z) f_i(v_\parallel(z)) dv_\parallel = N_e^2 R_{\text{ion}} dz_0. \tag{40}$$

Combining Eqs. (39) and (40) and imposing quasineutrality gives

$$\begin{aligned} N_e \exp\left(\frac{e\phi(z)}{T_e}\right) = \int dv_\parallel f_i(z, v_\parallel) &= \int_z^{L_z/2} \sqrt{\frac{m_i}{2e}} \frac{N_e^2 R_{\text{ion}}}{\sqrt{\phi(z_0) - \phi(z)}} dz_0 \\ &= \int_{\phi(z)}^{\phi(L_z/2)} \sqrt{\frac{m_i}{2e}} \frac{N_e^2 R_{\text{ion}}}{\sqrt{\phi(z_0) - \phi(z)}} \frac{dz_0}{d\phi(z_0)} d\phi(z_0), \end{aligned} \tag{41}$$

which is an implicit equation for $\phi(z)$. Setting our gauge so that $\phi(L_z/2) = 0$ and defining $x \doteq -e\phi(z_0)/T_e$ and $y \doteq -e\phi(z)/T_e$, we have

$$N_e \exp(-y) = \int_0^y \frac{h(x)}{\sqrt{y - x}} dx, \tag{42}$$

where

$$h(x) \doteq \frac{N_e^2 R_{\text{ion}}}{c_i} \frac{dz_0}{dx}. \tag{43}$$

The density integral appearing in Eq. (42) is of the form of an Abel transform [6], which can be inverted to yield

$$h(x) = \frac{N_e}{\pi} \frac{d}{dx} \int_0^x dy \frac{\exp(-y)}{\sqrt{x - y}} \tag{44}$$

Equating (43) and (44) yields an expression for dz/dx:

$$\frac{dz}{dx} = \frac{c_i}{N_e R_{\text{ion}} \pi} \frac{d}{dx} \int_0^x dy \frac{\exp(-y)}{\sqrt{x - y}}. \tag{45}$$

Integrating with respect to x yields an implicit expression for $\phi(z)$:

$$\begin{aligned} z - \frac{L_z}{2} &= \pm \frac{c_i}{\pi R_{\text{ion}} N_e} \int_0^x dy \frac{\exp(-y)}{\sqrt{x - y}} \\ &= \pm \frac{2c_i}{\pi R_{\text{ion}} N_e} D\left(\sqrt{-\frac{e\phi(z)}{T_e}}\right), \end{aligned} \tag{46}$$

with $D(a) = \exp(-a^2) \int_0^a \exp(b^2) db$ the Dawson function, the $+$ sign corresponds to $z > L_z/2$ and the $-$ sign corresponds to $z < L_z/2$.

4. Numerical implementation

A detailed description of the time and space discretisation employed in the code is given in [2], and the code itself is publicly available at `https://github.com/mabarnes/moment_kinetics`. Here we focus on the numerical treatment of the wall boundary conditions encapsulated in Eqs. (10)-(14).

Note that the boundary condition for the neutrals at $z = 0$ for $v_\parallel > 0$ depends on the neutral distribution function at $z = 0$ for $v_\parallel < 0$ through Γ_0. This distribution function requires specification of the neutral boundary condition for $z = L_z$ and $v_\parallel < 0$, which itself depends on the distribution function at $z = L_z$ for $v_\parallel > 0$. Due to the explicit time advance employed in the code, this inter-dependence is straightforward to accommodate.

The procedure employed is to first solve for $f_s(z, v_\parallel, t_{m+1})$ at all $(z, v_\parallel)$ locations except for $(z = 0, v_\parallel > 0)$ and $(z = L_z, v_\parallel < 0)$. As the time advance is explicit, this can be achieved given $\{f_s(z, v_\parallel, t_m)\}_{s=i,n}$. The solutions for $f_s(z = 0, v_\parallel < 0, t_{m+1})$ and $f_s(z = L_z, v_\parallel > 0, t_{m+1})$ are then used to compute $\Gamma_0(t_{m+1})$ and $\Gamma_{L_z}(t_{m+1})$. These fluxes can then be used in Eq. (11) to compute the boundary values $f_n(z = 0, v_\parallel > 0, t_{m+1})$ and $f_n(z = L_z, v_\parallel < 0, t_{m+1})$.

It is worth noting that in order to ensure the conservation of the field-line-averaged, species-summed density (as shown in Sec. 2.2), care must be taken to ensure that the properties $\int_0^\infty dv_\parallel v_\parallel f_{Kw} = -\int_{-\infty}^0 dv_\parallel v_\parallel f_{Kw} = 1$ are exactly satisfied by the numerics. This is achieved in our case by first obtaining the numerical approximation to these integrals and then defining a modified f_{Kw} that is normalised by this result.

5. Numerical results

We first compare our simulation results to the analytical solution presented in Sec. 3. The ion equation being solved in the code is

$$\frac{\partial \tilde{f}_i}{\partial \tilde{t}} + \tilde{v}_\parallel \frac{\partial \tilde{f}_i}{\partial \tilde{z}} - \frac{1}{2}\frac{\partial \tilde{\phi}}{\partial \tilde{z}}\frac{\partial \tilde{f}_i}{\partial \tilde{v}_\parallel} = \tilde{R}_{\text{ion}} \frac{c_i}{v_\delta} \exp\left(-\tilde{v}_\parallel^2 \frac{c_i^2}{v_\delta^2}\right), \tag{47}$$

where we have approximated $\delta(v_\parallel) \approx (1/\sqrt{\pi} v_\delta) \exp(-v_\parallel^2/v_\delta^2)$ with the proviso that $v_\delta \ll c_i$. In terms of normalised quantities, the solution (46) is

$$\tilde{z} = \frac{1}{2} \pm \frac{2}{\pi \tilde{R}_{\text{ion}}} D\left(\sqrt{-\tilde{\phi}}\right). \tag{48}$$

For our benchmark simulation, we use a Chebyshev pseudo-spectral method in both z and $v_\parallel$. The z grid consists of two z elements, each containing nine grid points, and the $v_\parallel$ grid consists of ten elements, each containing seventeen grid points. The wall temperature T_w is taken to be equal to T_e, the source width parameter is $v_\delta = 0.1 c_i$, $\tilde{R}_{\text{ion}} = 0.688$ and the ions are initialised to a Maxwellian velocity distribution with initial temperature T_e and an initial density with Gaussian distribution in z. The resulting

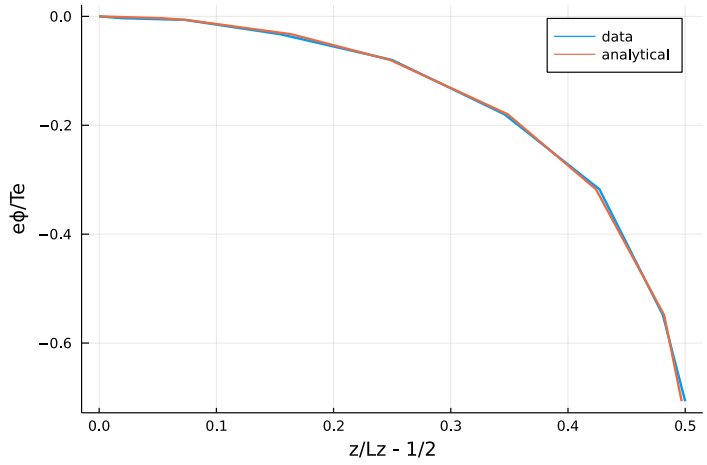

Figure 1. The steady-state electrostatic potential profile obtained by solving Eq. (47) (blue line) and by using the analytical solution of Eq. (46) (red line).

steady-state solution for $\tilde{\phi}(\tilde{z})$, along with a comparison to the analytical solution (48) is given in Fig. 1.

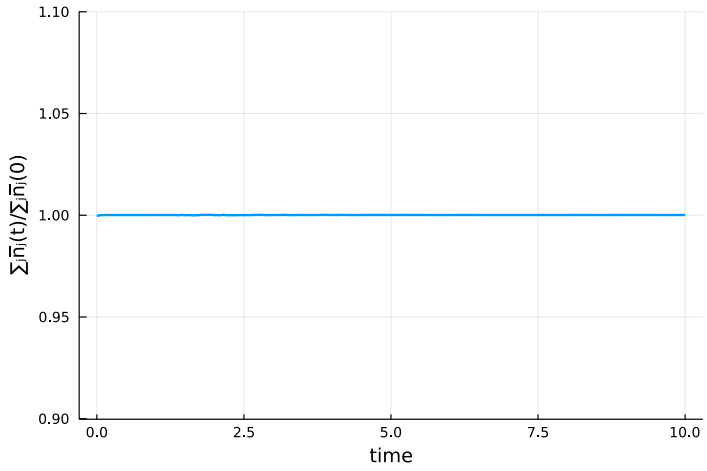

Figure 2. Time trace of the species-summed, line-averaged density, normalised by its initial value.

We next consider the original model system of equations given in Sec. 2.3. We take the normalised collision frequency factors to be $\tilde{R}_{\text{ion}} = \tilde{R}_{\text{in}} = 2$ and otherwise use the same numerical parameters and initial conditions as we did for the analytical benchmark, except that we use eight z elements rather than two. A cross-section of the numerical results are presented in Figures 2 - 4. In Fig. 2 we consider the evolution of the species-summed, line-averaged density. As shown in Sec. 3, this density should be conserved, and this is indeed the case in the simulation. The steady-state electrostatic potential and particle distribution functions for ions and neutrals are given in Figs. 3 and 4. As might be expected, the loss of electrons to the wall gives rise to an electric

field that pulls ions out of the simulation domain. These ions are replaced by neutrals traveling back into the simulation domain, leading to the regions of high neutral density near the walls (with neutral velocities away from the walls) visible in Fig. 4. The phase space structure in the ion distribution function is likely a result of the ionisation of neutrals in the high-density regions near the walls, followed by an acceleration of these ions towards the nearest wall. This reduces their initial speed away from the walls and eventually changes their direction of motion and accelerates them into the wall near which they were generated. Conversely, ions generated sufficiently far from the nearest wall can cross the symmetry point in z and are accelerated towards the wall furthest from where they were generated.

As an aside, we note that the kinetic Bohm criterion, which for the case of Boltzmann electrons can be written [5]

$$\int dv_\parallel \frac{c_i^2}{v_\parallel^2} f_i(v_\parallel) \leq 2n_i, \tag{49}$$

is satisfied for this simulation.

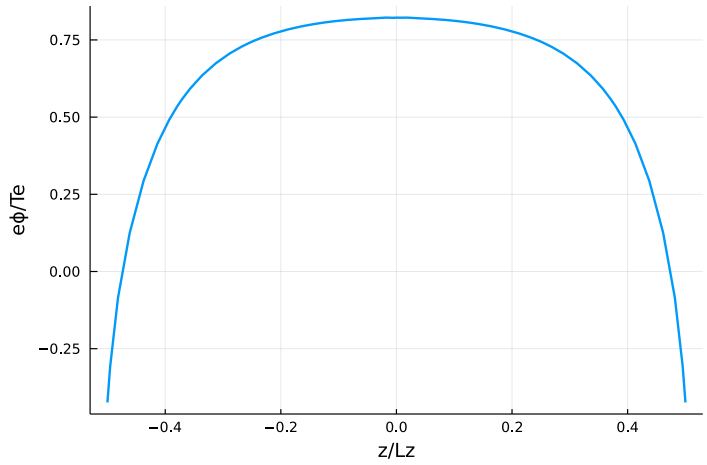

Figure 3. Electrostatic potential profile in steady state.

6. Future plans

Now that we have a working implementation of the standard drift kinetic equation with wall boundary conditions, we will move on to implementation of the wall boundary conditions for the moment-kinetic system of equations.

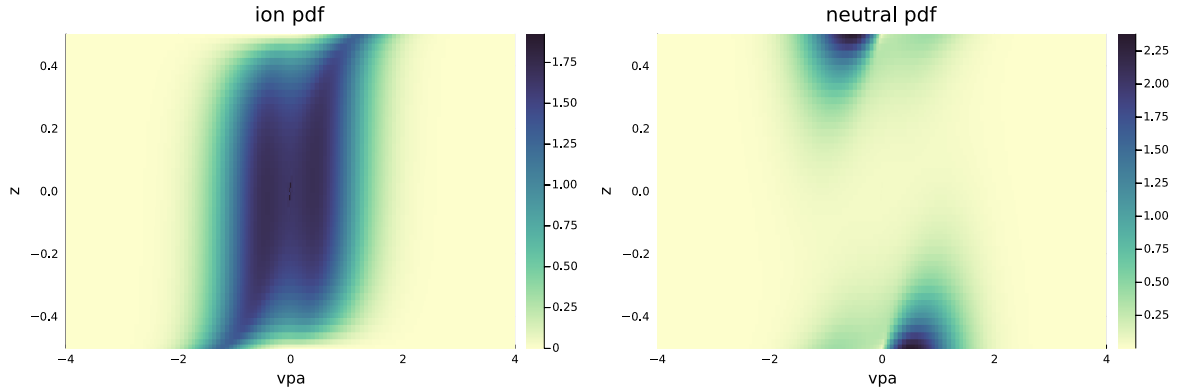

Figure 4. Phase space portraits of the steady-state, normalised ion (left) and neutral (right) particle distribution functions, $\tilde{f}_i$ and $\tilde{f}_n$.

[1] M. Barnes, F. I. Parra, and M. R. Hardman. Numerical study of 1d drift kinetic models with periodic boundary conditions. *Excalibur/Neptune Report*, 2:2047357–TN–01–02 M2.1, 2021.

[2] M. Barnes, F. I. Parra, M. R. Hardman, and J. Omotani. Numerical study of 1+1d, moment-based drift kinetic models with periodic boundary conditions. *Excalibur/Neptune Report*, 4:2047357–TN–01–02 M2.2, 2021.

[3] M. Barnes, F. I. Parra, M. R. Hardman, and J. Omotani. Numerical study of 1+1d, moment-based drift kinetic models with periodic boundary conditions. *Excalibur/Neptune Report*, 6:2047357–TN–01–02 M2.3, 2021.

[4] F. I. Parra, M. Barnes, and M. R. Hardman. 1d drift kinetic models with wall boundary conditions. *Excalibur/Neptune Report*, 5:2047357–TN–05–01 M1.3, 2021.

[5] E. R. Harrison and W. B. Thompson. The low pressure plane symmetric discharge. *Proc. Phys. Soc.*, 74:145, 1959.

[6] N. H. Abel. *Journal für die reine und angewandte Mathematik*, 1:153, 1826.